C Journal of Carbon Research

MDPI

Article

Self-Assembled Synthesis of Graphene Tubes from Melamine Catalyzed by Calcium Carbonate

Wenping Zeng [1], Jingxiang Meng [1], Xinbo Zheng [1], Tingting Mao [1], Jintao Huang [1,*] and Yonggang Min [1,2,*]

[1] School of Materials and Energy, Guangdong University of Technology, Guangzhou 510006, China; 1122302021@mail2.gdut.edu.cn (W.Z.); 2112302015@mail2.gdut.edu.cn (J.M.); 2112302229@mail2.gdut.edu.cn (X.Z.); 2112202194@mail2.gdut.edu.cn (T.M.)
[2] Huimai Material Technology (Guangdong) Co., Ltd., Foshan 528000, China
* Correspondence: jintao.huang@gdut.edu.cn (J.H.); ygmin@gdut.edu.cn (Y.M.)

Abstract: This study investigates the carbon products generated by melamine under various heat-treatment temperatures with the catalysis of calcium carbonate. We discovered that the cost-effective precursor melamine readily self-assembles and curls into graphene tubes when catalyzed by the alkaline earth salt $CaCO_3$ at elevated temperatures. Under heat-treatment conditions of 1100 °C and 1200 °C, the growth morphology of graphene tubes with open structures and exceptionally large diameters was observed, and the diameters reached the micron level. These products exhibit a high degree of carbonization and an extremely low nitrogen content, as low as 1.7%. Further, the intensity ratio (ID/IG) of the D band and the G band is as low as 0.79 in Raman characterization. The results show that the products have a certain graphite structure, which proves the catalytic activity of $CaCO_3$. This is attributed to the incorporation of $CaCO_3$ into the raw material system, which impedes the complete thermal decomposition of melamine. On the other hand, the resulting CaO particles are evenly distributed along the tubular products, providing certain support for their self-assembly and growth, thereby achieving the efficient growth of graphene tubes.

Keywords: melamine; calcium carbonate; graphene tubes; self-assembly; catalytic activity

Citation: Zeng, W.; Meng, J.; Zheng, X.; Mao, T.; Huang, J.; Min, Y. Self-Assembled Synthesis of Graphene Tubes from Melamine Catalyzed by Calcium Carbonate. *C* **2024**, *10*, 87. https://doi.org/10.3390/c10040087

Academic Editor: Gil Goncalves

Received: 31 July 2024
Revised: 13 September 2024
Accepted: 23 September 2024
Published: 26 September 2024

1. Introduction

The material known as graphene consists of sp^2 carbon atoms bonded in a honeycomb pattern, forming a two-dimensional structure [1–5]. The classification of a graphene tube occurs when one or multiple layers of graphene are curled into a tubular shape [6–8]. Therefore, tubular graphene structures, which combine the unique physical and chemical properties of two-dimensional graphene with the structural characteristics of one-dimensional hollows, hold a prominent position in the family of graphene nanostructures [9–11]. They possess great potential for applications in emission cathode materials, new energy batteries, sensors, supercapacitors, catalysts, and adsorption materials [12–15]. In particular, large-sized graphene tubes (GTs) offer a more expansive platform compared to carbon nanotubes as novel carriers for the advancement of oxygen reduction catalysts, facilitating the enhanced deposition of metal nanoparticles. Highly graphitized GTs exhibit robust interaction with catalyst nanoparticles and effectively prevent their aggregation, and the synergistic effect between GTs' carbon supports and metal nanoparticles contributes to the improved stability of the catalyst [16–18]. However, due to the limitations of the current preparation process, graphene tubes are generally synthesized through nucleation growth catalyzed by transition metals such as iron, cobalt, and nickel. This synthesis process necessitates additional post-treatments like template removal or acid leaching to obtain pure products. Consequently, challenges arise from expensive catalysts and lengthy preparation cycles [19–22]. Surprisingly, MoR et al. prepared graphene nanotubes with a high volume and energy density using alkaline earth metal oxide MgO nanowires as templates and catalysts by the CVD method, which could be used as anodes in lithium-ion batteries [23].

Recently, Luo et al. reported the template-free preparation of graphene tubes using calcium carbonate-catalyzed polyimide [24]. This statement is sufficient evidence to demonstrate the exceptional catalytic activity of alkaline earth metals and their oxides in the synthesis of graphene nanotubes, surpassing their role solely as carriers for transition metal catalysts such as iron, cobalt, and nickel [25–27].

Therefore, it is imperative to investigate a facile and high-yield approach for the synthesis of graphene tubes. Molecular self-assembly has emerged as a widely employed self-template strategy for fabricating nanostructured materials [28,29], in which melamine, as an excellent carbon-based material precursor, has attracted great interest from researchers [30–33]. For instance, nanotubes were synthesized via hydrothermal condensation using melamine as the precursor material, as demonstrated by Li et al. [34]. The nanotubes exhibited an outer diameter ranging from 70 to 200 nm, an inner diameter ranging from 5 to 20 nm, and a length of several microns. Similarly, Zhao et al. employed melamine as the sole precursor to facilitate the formation of self-assembling supramolecular intermediates via the hydrothermal method. Subsequently, these supramolecular intermediates were transformed into g-C_3N_4 nanotubes with abundant nitrogen defects through pyrolysis, which were utilized for efficient conversion of solar energy [35].

The self-assembly properties of melamine were exploited in this study to derive carbon products prepared under various temperature conditions through simultaneous heat treatment with the alkaline earth metal salt calcium carbonate, without the use of templates or transition metal catalysts. Particularly, the raw materials used in this study were limited to melamine and calcium carbonate, and the preparation process was relatively simple, involving only heat treatment of the raw materials. At a temperature of 1100 °C, tubular products with an evident open structure at the end and a pipe diameter reaching the micron level could be observed in the carbonized powder products. Importantly, after undergoing heat treatment at 1200 °C, the tubular products exhibited a more pronounced structure and a high degree of graphitization. Simultaneously, a significant amount of CaO particles, which were uniformly distributed along the growth direction of the tubular products, played a catalytic and supportive role in formation and growth, ultimately facilitating efficient graphene tube growth. Therefore, compared with the method of producing graphene tubes by transition metal catalysis, the method considered in this work has the characteristics of utilizing cheap raw materials and recyclable catalysts and constituting a simple process, which is of great significance for the industrial preparation of graphene tubes.

2. Materials and Methods

2.1. Material Synthesis

Using the low-cost industrial raw material melamine as a carbon source and nano-calcium carbonate as a catalyst, graphene tubes were synthesized in a high-temperature environment. The raw materials were sourced from Shanghai Maclin Co., Ltd. (Shanghai, China). Pure melamine and nano-calcium carbonate (with a particle size of 50 nm) powder were finely ground in a quartz mortar to create a homogeneous mixture, and the content of $CaCO_3$ in the feedstock system was 20 wt%. Subsequently, the raw materials were placed into a graphite mold within a tube furnace and experimental heat-treatment groups were established at 800 °C, 900 °C, 1000 °C, 1100 °C, and 1200 °C in N_2, with a heating rate of 10 °C/min. Before heating, the furnace was purged three times with high-purity argon using a rotary vacuum pump to reduce the O_2 concentration to a negligible level. Then, the heating process was initiated, and once the temperature reached the designated level, it was maintained for a duration of 30 min before natural cooling to produce the final carbon product.

2.2. Material Characterization

The morphology of the product was characterized using SEM and elemental mapping with a Hitachi SU8010 microscope (Hitachi Inc., Tokyo, Japan) equipped with energy disper-

sive X-ray spectroscopy (EDS) equipment. The METTLER TGA2 (METTLER TOLEDO Inc., Zurich, Switzerland) was used to analyze the thermal stability of the raw materials in N_2 with a heating rate of 20 °C/min. XPS was performed using the Thermo Scientific K-Alpha X-ray (Thermo Fisher Inc., Waltham, MA, USA) photoelectron spectrometer system with a monochromatic Al K-Alpha source operated at 150 eV for full-spectrum scanning and 50 eV for narrow-spectrum scanning. Phase identification was performed using XRD on a Rigaku Ultima IV diffractometer (Rigaku Inc., Tokyo, Japan) with Cu K-Alpha X-rays. Raman spectra were tested using a LabRam HR Evolution Micro confocal Raman spectrometer (HORIBA Jobin Yvon Inc., Paris, France) with an excitation wavelength of 532 nm. Samples were prepared as powders on a glass surface, with the excitation laser focused through a 100× microscope objective for a total interrogation spot size of ~1 micron diameter. The FT-IR spectroscopy of Nicolet6700 (Thermo Fisher Inc., Waltham, MA, USA) was used for infrared absorbance spectroscopy measurement.

3. Results

3.1. Microscopic Morphology of Carbon Products

The industrial raw materials used in this paper were melamine powder with a particle size of microns and nano-calcium carbonate (Supplementary Materials, Figure S1). The raw materials were mixed evenly by grinding, resulting in numerous calcium carbonate particles embedded in the surface of the melamine, which provided a basis for the subsequent CaO particles to coat the graphene tube products, as shown in Figure 1a.

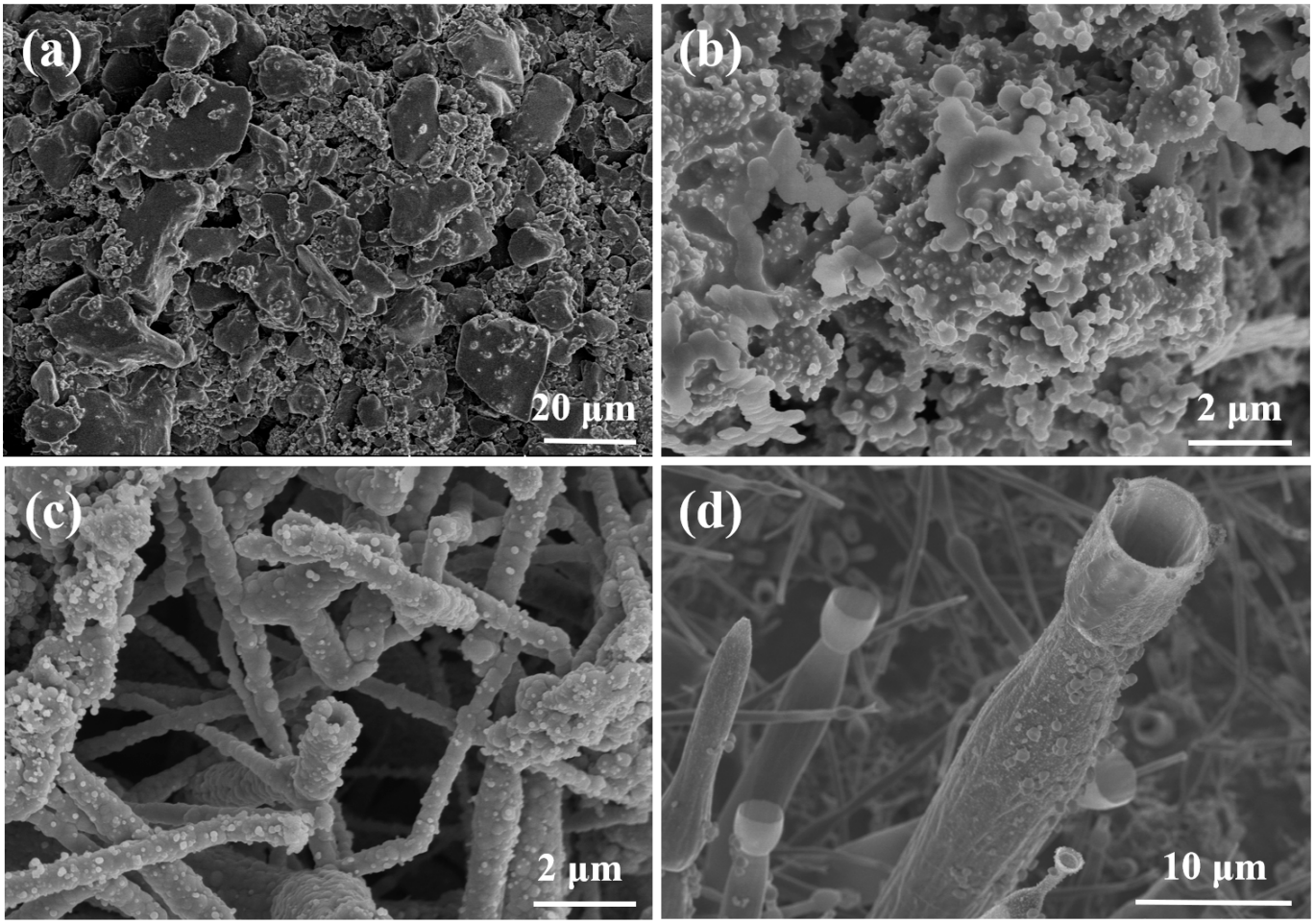

Figure 1. SEM images of (**a**) the raw material system and the carbon products obtained with different heat-treatment temperatures: (**b**) 1000 °C, (**c**) 1100 °C, and (**d**) 1200 °C.

In the experiments with different temperatures, the carbon products predominantly existed in blocky or layered structures when the heat-treatment temperature was below 1000 °C, as shown in Figure 1b, which illustrates the morphology of the products from the 1000 °C heat-treatment group. This was primarily due to the energy from the external environment being insufficient to transform the graphene sheets into rolled tube structures. Until the heat-treatment temperature reached 1100 °C, thick-walled tubular products (external diameters of 1–2 μm and open-ended) were observed in the black powder product, and numerous spherical granular materials were uniformly distributed outside the tube walls (Figure 1c). Furthermore, when the heating temperature was 1200 °C, as shown in Figure 1d, the growth morphology of tubular products with larger diameters and hollow structures could be observed. The maximum diameter of the tubes was close to 10 μm, the length of the tubes was uneven, and the wall thickness of the tubes was about several hundred nanometers. In addition, the tubular products grew in situ, segment by segment, like bamboo shoots, which is a direct demonstration of the mechanism of tube growth. Unfortunately, only incomplete tubular products were observed in the powder product, which could possibly be attributed to the substantial diameters and hollow structures of the tubes, causing egress of the fully developed tubular products from the reaction mold due to their exceedingly low mass. In a word, the diameters and growth mode of the observed tubes in this study differed significantly from those of traditional nanotubes. Consequently, the tube structures investigated in this experiment were designated graphene tubes (GTs), as supported by relevant reports in the literature [24].

3.2. Mechanism of Tube Formation

To gain further insight into the elemental composition of the products and elucidate the mechanism of tube formation, X-ray elemental energy spectrum analysis was conducted on the products in the experimental groups at 1100 °C and 1200 °C using scanning electron microscopy, as depicted in Figure 2. The even distribution of C, N, O, and Ca elements along the tubular products was evident. The mass fraction of each element is depicted in Figure S2, illustrating that CaO particles uniformly adhered to the outer walls of the tubes. It should be noted that the N element content was minimal, indicating that carbon tubes primarily constitute the tubular structure observed in the SEM photos. The CaO particles distributed outside the tubes are believed to serve as temporary supports during the self-assembly process of the tube structures, mainly catalyzing the formation of the initial tube structures, thereby preventing the disordered growth and intertwining of the tube structures and facilitating the growth of the tubular structures section by section. Subsequently, the CaO particles naturally fall off, and Figure 1d also shows an image of a tube structure without CaO attached to the tube wall.

Based on the above analysis, we propose that the catalytic mechanism of CaO in promoting GT formation is different from the top growth or bottom growth of carbon nanotubes catalyzed by transition metals. However, CaO particles serve as a support for the initial tubular structure by attaching to the wall of GTs. Additionally, CO_2 products decomposed by $CaCO_3$ at high temperatures act as etching agents for amorphous carbon. This process reduces the degree of defects in carbon products and ultimately yields highly graphitized tubular structures. Therefore, the diameters of the GTs grown in this experiment remained unaffected by the catalyst particle size. This observation provides a comprehensive explanation of the occurrence of GTs with exceptionally large diameters observed in this study. Furthermore, through EDS spectrum data (Figure S2) and subsequent XPS analysis, it can be conclusively demonstrated that the tubular structures formed were not derived from g-C_3N_4 tubes. Instead, under high-temperature conditions and calcium-based catalysis, multiple layers of graphene underwent curling to form these distinctive GTs.

We conducted a thermal stability analysis of the raw materials to study the effect of $CaCO_3$ on the thermal decomposition process of melamine, which is crucial to elucidate the growth mechanism of the tubular products. Therefore, we performed a TGA analysis

on the raw material system and compared it with a control experiment. The weight loss curves of the raw material system containing $CaCO_3$ and the pure melamine raw material were compared, as depicted in Figure 3a. It can be observed that the weight loss occurring within the temperature range of 250−373 °C is primarily attributable to the decomposition of melamine. Both systems exhibit similar decomposition rates; however, the sample containing $CaCO_3$ exhibits a slightly advanced mass loss behavior, with an 8 °C temperature difference when the raw material's weight loss reaches 20%.

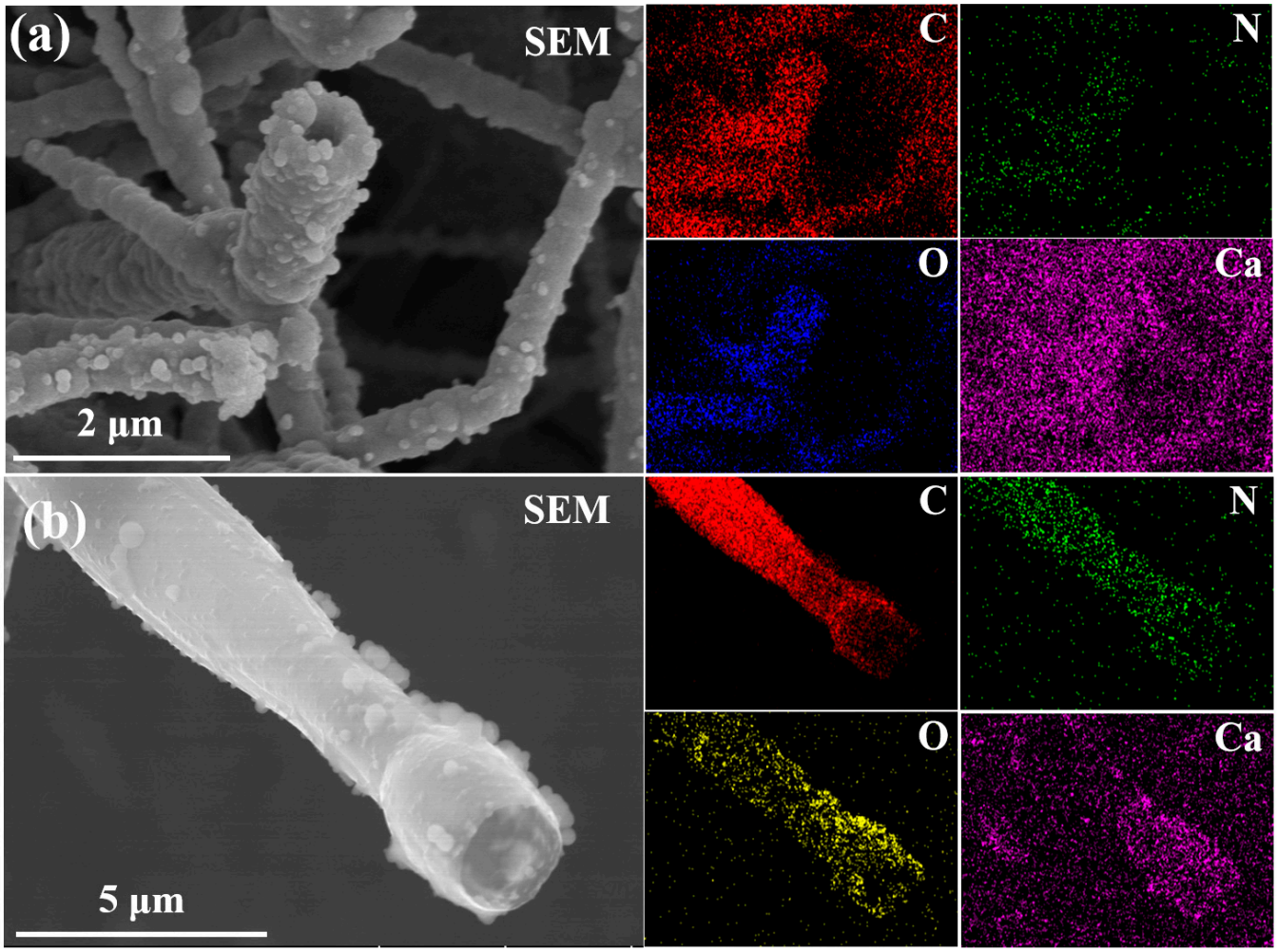

Figure 2. SEM images of various GTs and corresponding C, N, O, and Ca element mapping spectra with different heat-treatment temperatures: (**a**) 1100 °C and (**b**) 1200 °C.

Furthermore, the $CaCO_3$/melamine sample exhibited a 7% mass loss within the temperature range of 625–724 °C, which can be attributed to the high-temperature decomposition reaction of $CaCO_3$ into CaO and CO_2. This mass loss corresponds to the weight of CO_2 released. Based on calculations, if we consider the weight loss of CaO as well, the total weight loss of the final mixed material should be 93%. In comparison with pure melamine, there was a significant reduction in weight loss (97%) at 724 °C. Therefore, incorporating $CaCO_3$ into the mixed raw material can partially mitigate the complete thermal decomposition of melamine. As the temperature increases, decomposed solid CaO particles from $CaCO_3$ catalyze the self-assembly growth of melamine molecules to form graphene tubes (GTs), which attach themselves onto the outer surfaces of the initially formed tube structures as supports. This is why the pure melamine sample began to decompose twice after 900 °C and completely decomposed at 1050 °C, while the raw material system containing

$CaCO_3$ did not decompose again after 900 °C. This stage corresponds to the formation of GTs under the catalytic action of the calcium group.

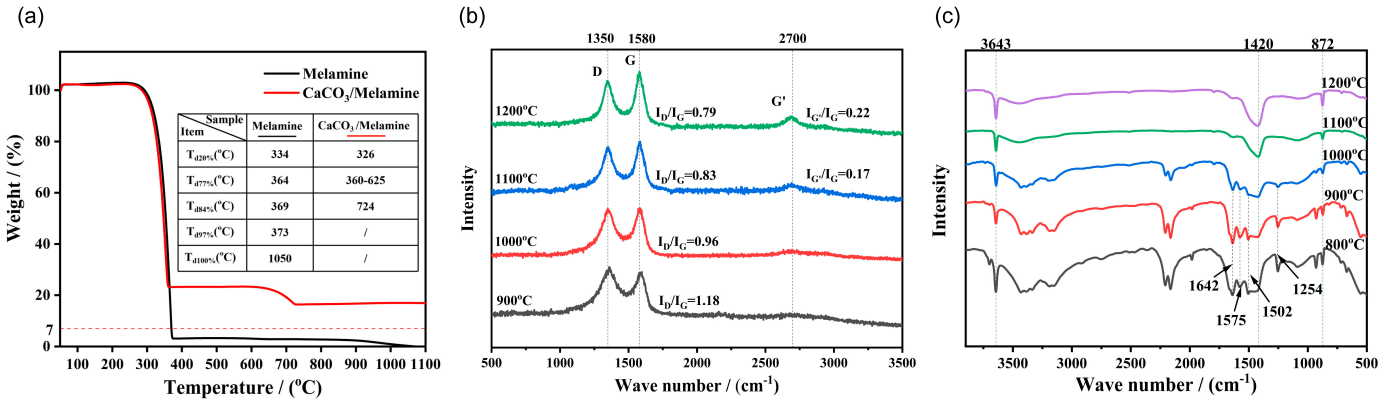

Item \ Sample	Melamine	$CaCO_3$/Melamine
$T_{d20\%}$(°C)	334	326
$T_{d77\%}$(°C)	364	360-625
$T_{d84\%}$(°C)	369	724
$T_{d97\%}$(°C)	373	/
$T_{d100\%}$(°C)	1050	/

Figure 3. (**a**) TGA curves and corresponding TGA characteristic thermal data of the $CaCO_3$/melamine and melamine samples. (**b**) Raman spectra of the powder product obtained at 900–1200 °C. (**c**) FT-IR spectra of the powder product obtained at 800–1200 °C.

3.3. Characterization of Carbon Products

To determine the elemental composition and structure of the products, we characterized the products obtained at 800 °C and 1200 °C by X-ray photoelectron spectroscopy (XPS) and the XPS survey spectra of the carbon products, as shown in Figure S3. The XPS survey spectra for the products obtained at 800 °C and 1200 °C show characteristic peaks for C, N, O, and Ca. The peak at around 284.8 eV corresponds to the C1s peak, the peak at around 401 eV corresponds to the N1s peak, the peak at around 532 eV corresponds to the O1s peak, and the peak at around 350 eV corresponds to the Ca2p peak, indicating that the products contained C, N, O, and Ca elements. However, due to the variations in heat-treatment temperatures, there were significant differences in the relative mass fractions of the elements. Figure S4 (Supplementary Materials) presents a summary of the relative mass fractions for each element; under 800 °C heat-treatment conditions, carbonization was limited, and the resulting product still contained a substantial amount of nitrogen. Conversely, under 1200 °C heat-treatment conditions, carbonization was extensive and only trace amounts of nitrogen remained in the product. These findings suggest that during carbonization, carbon atoms undergo rearrangement while simultaneously losing nitrogen content, leading to the formation of a multilayer graphene structure that further self-assembles into tubular structures by curling from lamellar arrangements. Therefore, when the heat-treatment temperature reaches 1200 °C, there is a significant increase in carbon content in the product, indicating a substantial conversion of melamine into graphene tube products. Meanwhile, the nitrogen content remains minimal, suggesting the breakage of C-N bonds and the rearrangement of carbon atoms instead of continuous pyrolysis into small-molecule spill molds at 800 °C. The findings demonstrate that both high temperatures and catalytic action in calcium-based catalysis can enhance the yield of carbon products.

The partial peak fitting of C1s in Figure 4a reveals the presence of three distinct C1s peaks, with the dominant contribution arising from sp^2 hybrid carbon at 284.8 eV, while the peaks at 285.3 eV originate from unconverted sp^3 hybrid carbon (C-N) and a minor fraction of C-O [24]. The distinction lies in the fact that, following heat treatment at 1200 °C, the C1s satellite peak fitted by 290.42 eV predominantly corresponds to the π-π^* interaction between distinct carbon components or different graphene layers within the GTs, indicating a high level of carbonization and a certain graphite structure in the sample [14]. This observation aligns with the remarkably elevated carbon content. Similarly, as depicted in Figure 4b of the N1s sub-peak fitting diagram, the presence of nitrogen in carbon products subjected to heat treatment at 800 °C is primarily attributable to C-N configurations, resulting in a relatively high nitrogen content. Conversely, upon heat treatment at 1200 °C, nitrogen

exists in carbon products through heteroatom doping. The high-resolution N1s spectrum reveals fitted peaks at 398.49 eV and 401.6 eV corresponding to pyridinic and graphitic nitrogen, respectively [36], with an extremely low nitrogen content of only 1.7% observed (Figure S4). Further, the peak fitting data based on the high-resolution N1s spectrum shows that the ratio of pyridinic N and graphitic N is about 1:1. The fine spectra of O and Ca elements also demonstrate distinct compositional and structural differences in the high graphitization structure and carbon mass fraction increase after heat treatment at 1200 °C as compared to that at 800 °C (Figure S5). As the temperature increases and the graphene tube structure grows, the carbon product gradually separates from the calcium-based catalyst, resulting in an increase in the carbon content of the product, so the signal of the O and Ca elements shown in Figure S5 is weaker. In general, based on the TGA and XPS analyses conducted above, it can be observed that while calcium carbonate can undergo complete decomposition into CaO particles under the heat-treatment condition of 800 °C, this temperature is insufficient to provide the necessary energy for self-assembly and coiling of flake graphene structures, thereby hindering the successful growth of graphene tubes. Hence, it is evident that the generation of graphene tubes in this study cannot solely have relied on the decomposition temperature of calcium carbonate but also required an appropriate temperature for flake graphene self-assembly, that is, these two factors are indispensable for the growth of GTs.

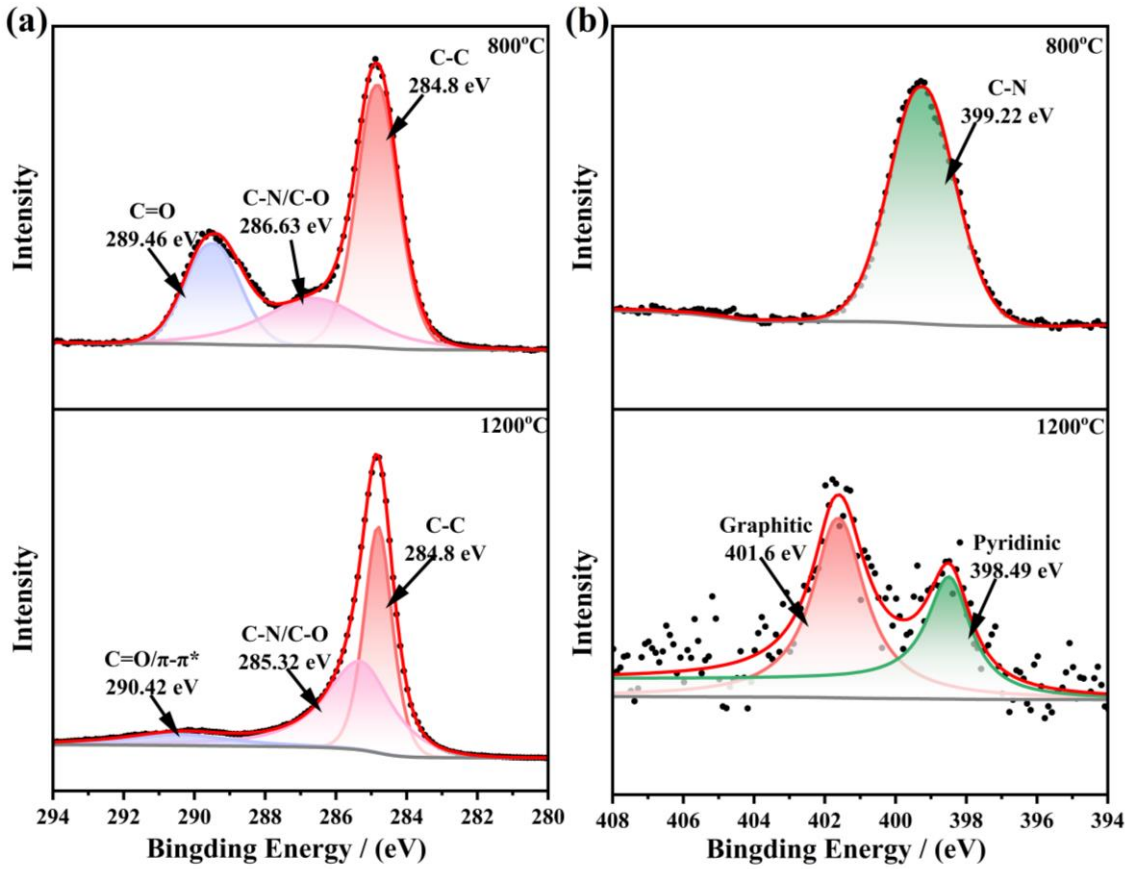

Figure 4. (**a**) C1s high-resolution XPS spectra and (**b**) N1s high-resolution XPS spectra of the carbon products obtained at 800 °C and 1200 °C.

The component crystal phase of the product was determined using powder X-ray diffraction (XRD). As depicted in Figure 5a, the XRD patterns of the products under all temperature conditions exhibited no presence of metal carbides or elemental peaks. Hence, there was no occurrence of metal carburization resulting from carbon-source decomposition, thereby catalyzing carbon nanotube growth. This indicates that the formation

mechanism of GTs in this experiment differs entirely from that based on transition metal catalysis. We observed that the calcium-based products in the samples predominantly exhibited the characteristic peak of $Ca(OH)_2$, and the peak values and peak positions were completely consistent with the standard spectrum (PDF#00-044-1481). This consistency can be attributed to the facile adsorption and conversion of CaO from atmospheric water. Due to the influence of the diffraction peak from the calcium-based product, the characteristic peak of the carbon product was not prominently discernible. Therefore, Figure 5b shows a locally amplified diffraction pattern in the range of 25–28° with 2θ. The carbon products below 1000 °C exhibit two characteristic peaks at 26.4° and 26.7°, respectively, indicating a low degree of graphitization, resulting in differentiation and migration of the graphite (002) peak. As the temperature rises to 1100 °C and above, the prominent main peak of graphite (002) near 26.5° suggests an increased degree of graphitization in carbon products, leading to narrower diffraction peak shapes. The (002) diffraction peak of graphite at 1200 °C can be observed at 26.43°, while the single-walled carbon nanotubes exhibit a peak around 26.5°, which can possibly be attributed to the leftward shift caused by an increased number of graphene tube layers [24]. Further calculation using the Mering–Maire formula reveals that the crystal face spacing of graphite layers is approximately 0.34 nm [37]. This further confirms that the tubular structure present in the product is composed of graphene tubes.

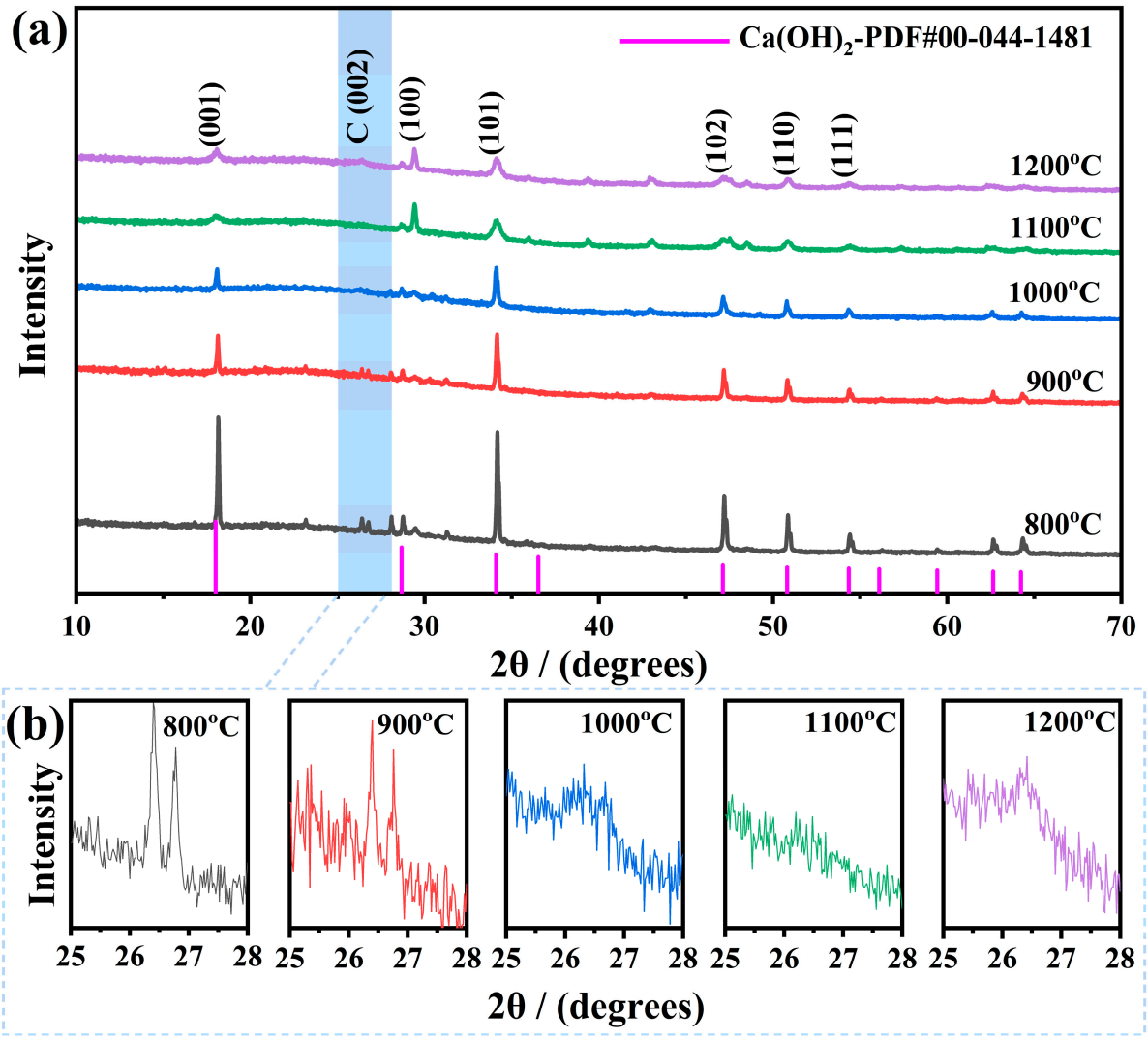

Figure 5. (**a**) XRD patterns of the powder product obtained at 800–1200 °C. (**b**) The corresponding 2θ is a locally amplified diffraction pattern in the range of 25–28°.

Raman spectral analysis was conducted to characterize the structure and quality of the carbon products, and the results are presented in Figure 3b. Under excitation at 532 nm, Raman spectra within the frequency range of 500–3500 cm^{-1} were acquired, revealing prominent first-order peaks in the G band (~1580 cm^{-1}) and the D band (~1350 cm^{-1}), indicating the presence of highly graphitized carbons with diverse defects resulting from nitrogen incorporation and other potential imperfections [38]. It is worth noting that within the temperature range of 900–1200 °C, the intensity ratio (I_D/I_G) between the D band and the G band gradually decreased with increasing temperature. This observation indicates a reduction in internal defects, an enhancement in carbon atom arrangement, and an increase in graphitization degree. However, at 800 °C, the product exhibited a low carbonization degree without any characteristic peak. Additionally, following the temperature increase to 1100 °C, all samples exhibited a secondary peak around 2700 cm^{-1}, corresponding to the 2D or G′ band [39]. It has been reported that the intensity ratio of the G′ band to the G band ($I_{G'}/I_G$) serves as an effective method for characterizing graphene or carbon nanotube thickness, with a lower $I_{G'}/I_G$ value indicating relatively thicker graphene tubes. Therefore, it can be inferred that the graphene tube product formed at 1100 °C possesses greater thickness compared to that formed at 1200 °C, which aligns with the microscopic image of GTs observed via SEM. The heat-treatment condition of 1200 °C may serve as the critical temperature for the growth of graphene tubes and the rearrangement of carbon atoms, as indicated by the observed trends in XRD and Raman spectra. This temperature corresponds to a significant abundance of lamellar graphene self-assembling into coiled tube structures. Moreover, temperatures below 1200 °C necessitate prolonged holding times to provide continuous energy for enabling extensive curling of lamellar graphene into tubes.

The Fourier transform infrared spectra of carbon products were depicted in Figure 3c, all samples showed strong sharp bands near 3643 cm^{-1}, which were attributed to the O-H stretching pattern of $Ca(OH)_2$. That is to say, the CaO in the product easily absorbs water vapor in the air to form $Ca(OH)_2$, which is consistent with the phenomenon observed in the XRD pattern. The other two bands at 1420 cm^{-1} and 872 cm^{-1} belong to the corresponding carbonate groups [40], indicating that part of $Ca(OH)_2$ absorbs CO_2 from the air to form carbonate. For carbon products, we found that the IR spectra below 1000 °C were consistent. The observed absorption bands at approximately 1254, 1502, 1575, and 1642 cm^{-1} are indicative of the characteristic stretching vibration modes associated with CN heterocycles [41]. This suggests a higher nitrogen content and the presence of C-N heterocycles within the carbon products. The absorption peak of 2000–2400 cm^{-1} corresponds to nitrile groups [42]. Upon reaching a temperature of 1100 °C, an increased degree of carbonization can be observed, along with a reduction in nitrogen content and the disappearance of the corresponding absorption peaks of C-N and nitrile groups. Therefore, the carbon products were mainly divided into C elements, but the absorption peaks were not obvious due to the influence of calcium compounds in the products. In particular, the absence of a spectral band at approximately 812 cm^{-1} corresponding to the characteristic respiratory mode of the S-triazine unit was observed in all products [43]. This observation suggests that the carbon products obtained after high-temperature heat treatment differ from g-C_3N_4 nanotubes and that the tubular products grown at 1100 °C and 1200 °C are highly graphitized graphene tubes. These findings align with the results indicating extremely low nitrogen contents in both the EDS and XPS spectra. In addition, the products at temperatures below 1000 °C show a wide vibration band near 3000–3600 cm^{-1}, which corresponds to the surface-bound H_2O molecules and amino groups, indicating that the carbon products containing N have an expanded open surface [44]. The highly graphitized carbon nanotube products obtained after 1100 °C and 1200 °C heat treatment showed unique hydrophobic phenomena and chemical inertness, resulting in the disappearance of corresponding absorption peaks [45].

4. Discussion

In this study, a temperature-gradient experiment was conducted in the range of 800−1200 °C using a mixture of melamine and calcium carbonate as raw materials. The microscopic morphology of graphene tube growth was observed at both 1100 °C and 1200 °C. The diameters of the tubular products were significantly larger than those of carbon nanotubes, with an evident open structure at the end, indicating a higher degree of graphitization. Additionally, a layer of CaO particles uniformly adhered to the incomplete tube walls as a support, confirming the catalytic effect of the alkaline earth metal salt calcium carbonate on tubular product growth. Then, TGA thermogravimetric analysis of the raw materials was conducted to verify the catalytic effect of $CaCO_3$ on melamine cracking, while XPS, XRD, Raman, and FT-IR characterizations were performed to further confirm the high degree of graphitization in the resulting tubular structures, primarily attributed to graphene crimping. Therefore, we propose a mechanism in which calcium carbonate acts as a catalyst for the self-assembly of melamine, resulting in the formation of GTs. The presence of $CaCO_3$ particles in the raw materials effectively inhibits the complete thermal decomposition of melamine. Additionally, CaO, generated through high-temperature decomposition, catalyzes the self-assembly and coiling of melamine cracking intermediate products to form GTs while providing structural support during their initial morphological development. This sequential growth process resembles that of bamboo shoots emerging one by one. Furthermore, the CO_2 gas released from the decomposition of $CaCO_3$ at high temperatures serves as an etching agent for amorphous carbon, preventing its accumulation and enhancing the efficiency of graphene tube generation.

The catalyst can be reused throughout the reaction system due to the growth mechanism of GTs and the high-temperature stability of CaO, making it a cost-effective option compared to other transition metals produced by metal carburizing GTs. Additionally, the catalyst is easily recyclable, and the process is straightforward. Subsequent efforts will focus on optimizing experimental conditions and process parameters, such as prolonging the holding time, adjusting raw material particle size to achieve controllable dimensions of GTs, and establishing separate reactors for raw materials and collectors for products. These measures will aim to efficiently gather fully developed high-purity GTs while enabling catalyst reuse, thereby truly realizing a simple, effective, and environmentally friendly approach that provides a fresh method for industrial-scale production of graphene tube products.

5. Conclusions

The present study aimed to investigate the one-step preparation of graphene tubes using cost-effective industrial raw materials, namely, melamine and alkaline earth metal salt calcium carbonate, through a simplified heat-treatment process. This approach offers significant simplification compared to hydrothermal or chemical vapor deposition (CVD) methods, while also reducing the raw material costs associated with expensive transition metal catalysts. In the experimental practice, the facile self-assembly characteristics of melamine were ingeniously combined with the catalytic activity of alkaline earth metals. By optimizing the process and adjusting parameters such as temperature, we successfully observed the growth morphology of graphene tubes. This verified both the feasibility of the raw materials and the preparation technology, leading to the proposal of a novel mechanism for the catalysis of graphene tube growth by calcium compounds. In a word, this work offers a novel concept and research foundation for the investigation of alkaline earth metal salts or compounds as catalysts for the growth of self-assembled graphene tubes from easily accessible substances.

Supplementary Materials: The following supporting information can be downloaded at: https://www.mdpi.com/article/10.3390/c10040087/s1, Figure S1: SEM images of (a) pure melamine and (b) nano-calcium carbonate; Figure S2: EDS spectra of the GT surfaces of carbon products obtained at 1100 °C; Figure S3: XPS survey spectra of the carbon products obtained at (a) 800 °C and (b) 1200 °C; Figure S4: Elemental quantification results obtained from XPS analysis for the carbon products obtained at 800 °C and 1200 °C; Figure S5: (a) O1s high-resolution XPS spectra and (b) Ca2p high-resolution XPS spectra of the carbon products obtained at 800 °C and 1200 °C.

Author Contributions: W.Z.: Conceptualization, investigation, and writing—original draft preparation. J.M.: Methodology. X.Z.: Data curation. T.M.: Validation and formal analysis. J.H.: Funding acquisition, visualization, and writing—review and editing. Y.M.: Project administration and supervision. All authors have read and agreed to the published version of the manuscript.

Funding: This research was funded by the National Natural Science Foundation of China (Grant Nos. 52003111, 21975054, and U20A20340), the National Key R&D Program of China (2020YFB0408100), the Anhui Provincial Key Research and Development Project (2023z04020021), the Program for Guangdong Introducing Innovative and Entrepreneurial Team (2016ZT06C412), and the Foshan Science and Technology Innovation Team Project (1920001000108).

Data Availability Statement: Data will be made available on request.

Conflicts of Interest: Author Yonggang Min was employed by the company Huimai Material Technology (Guangdong) Co., Ltd. The remaining authors declare that the research was conducted in the absence of any commercial or financial relationships that could be construed as a potential conflict of interest.

References

1. Novoselov, K.S.; Geim, A.K.; Morozov, S.V.; Jiang, D.; Zhang, Y.; Dubonos, S.V.; Grigorieva, I.V.; Firsov, A.A. Electric Field Effect in Atomically Thin Carbon Films. *Science* **2004**, *306*, 666–669. [CrossRef] [PubMed]
2. Wang, X.; Lim, E.G.; Hoettges, K.; Song, P. A Review of Carbon Nanotubes, Graphene and Nanodiamond Based Strain Sensor in Harsh Environments. *C* **2023**, *9*, 108. [CrossRef]
3. He, X.; Cui, C.; Chen, Y.; Zhang, L.; Sheng, X.; Xie, D. MXene and Polymer Collision: Sparking the Future of High-Performance Multifunctional Coatings. *Adv. Funct. Mater.* **2024**, 2409675. [CrossRef]
4. Xu, W.; Yang, W.; Su, J.; Huang, J.; Min, Y.; Yu, Y.; Zeng, Y.; Chen, P.; Wang, Y.; Li, X. Diatom-Based Biomass Composites Phase Change Materials with High Thermal Conductivity for Battery Thermal Management. *J. Energy Storage* **2024**, *96*, 112737. [CrossRef]
5. Chen, Y.-C.; Jiang, X.-Y.; Thanh, B.X.; Lin, J.-Y.; Wang, H.; Huang, C.-W.; Yang, H.; Ebrahimi, A.; Sirivithayapakorn, S.; Lin, K.-Y. Magnetic Carbon Foam Adorned with Co/Fe Nanoneedles as an Efficient Activator of Oxone for Oxidative Environmental Remediation: Roles of Surficial and Chemical Enhancement. *C* **2023**, *9*, 107. [CrossRef]
6. Jiao, L.; Zhang, L.; Wang, X.; Diankov, G.; Dai, H. Narrow Graphene Nanoribbons from Carbon Nanotubes. *Nature* **2009**, *458*, 877–880. [CrossRef]
7. Li, Q.; Xu, P.; Gao, W.; Ma, S.; Zhang, G.; Cao, R.; Cho, J.; Wang, H.; Wu, G. Graphene/Graphene-Tube Nanocomposites Templated from Cage-Containing Metal-Organic Frameworks for Oxygen Reduction in Li-O2 Batteries. *Adv. Mater.* **2014**, *26*, 1378–1386. [CrossRef]
8. Song, G.; Li, Z.; Meng, A.; Zhang, M.; Li, K.; Zhu, K. Large-Scale Template-Free Synthesis of N-Doped Graphene Nanotubes and N-Doped SiO2-Coated Graphene Nanotubes: Growth Mechanism and Field-Emission Property. *J. Alloys Compd.* **2017**, *706*, 147–155. [CrossRef]
9. Verma, A.K.; Singh, J.; Nguyen-Tri, P. Gold-Deposited Graphene Nanosheets for Self-Cleaning Graphene Surface-Enhanced Raman Spectroscopy with Superior Charge-Transfer Contribution. *ACS Appl. Mater. Interfaces* **2024**, *16*, 10969–10983. [CrossRef]
10. Khezami, L.; Aissa, M.A.B.; Modwi, A.; Ismail, M.; Guesmi, A.; Algethami, F.K.; Ticha, M.B.; Assadim, A.A.; Nguyen-Tri, P. Harmonizing the Photocatalytic Activity of g-C_3N_4 Nanosheets by ZrO_2 Stuffing: From Fabrication to Experimental Study for The Wastewater Treatment. *Biochem. Eng. J.* **2022**, *182*, 108411. [CrossRef]
11. Jiang, H.; Li, J.; Xie, Y.; Guo, H.; He, M.; Shi, X.; Mei, Y.; Sheng, X.; Xie, D. Design of Efficient Microstructured Path by Magnetic Orientation Boron Nitride Nanosheets/$MnFe_2O_4$ Enabling Waterborne Polyurethane with High Thermal Conductivity and Flame Retardancy. *J. Mater. Sci. Technol.* **2025**, *209*, 207–218. [CrossRef]
12. Wang, R.; Hao, Y.; Wang, Z.; Gong, H.; Thong, J.T.L. Large-Diameter Graphene Nanotubes Synthesized Using Ni Nanowire Templates. *Nano Lett.* **2010**, *10*, 4844–4850. [CrossRef] [PubMed]
13. Zhang, Y.; Tan, Y.-W.; Stormer, H.L.; Kim, P. Experimental Observation of the Quantum Hall Effect and Berry's Phase in Graphene. *Nature* **2005**, *438*, 201–204. [CrossRef]

14. Gupta, S.; Qiao, L.; Zhao, S.; Xu, H.; Lin, Y.; Devaguptapu, S.V.; Wang, X.; Swihart, M.T.; Wu, G. Highly Active and Stable Graphene Tubes Decorated with FeCoNi Alloy Nanoparticles via a Template-Free Graphitization for Bifunctional Oxygen Reduction and Evolution. *Adv. Energy Mater.* **2016**, *6*, 1601198. [CrossRef]
15. Chen, M.; Hwang, S.; Li, J.; Karakalos, S.; Chen, K.; He, Y.; Mukherjee, S.; Su, D.; Wu, G. Pt Alloy Nanoparticles Decorated on Large-Size Nitrogen-Doped Graphene Tubes for Highly Stable Oxygen-Reduction Catalysts. *Nanoscale* **2018**, *10*, 17318–17326. [CrossRef] [PubMed]
16. Majidi, R. Structural and Electronic Properties of S-Graphene Nanotubes: A Density Functional Theory Study. *Diam. Relat. Mater.* **2021**, *118*, 108520. [CrossRef]
17. Li, Q.; Pan, H.; Higgins, D.; Cao, R.; Zhang, G.; Lv, H.; Wu, K.; Cho, J.; Wu, G. Metal–Organic Framework-Derived Bamboo-like Nitrogen-Doped Graphene Tubes as an Active Matrix for Hybrid Oxygen-Reduction Electrocatalysts. *Small* **2015**, *11*, 1443–1452. [CrossRef]
18. Song, G.; Luo, S.; Zhang, J.; Zhang, M.; Qiu, G.; Meng, A.; Lin, Y.; Li, Z. Template-Free One-Step Synthesis of the Multi-Layer Carbon or Stacked Graphene Sheets Coessentially Coating N-Doped Graphene Tubes and Their Field Emission and Photoluminescence Properties. *J. Alloys Compd.* **2020**, *829*, 154411. [CrossRef]
19. Wang, Q.; Zhang, L. Fabricated Ultrathin Magnetic Nitrogen Doped Graphene Tube as Efficient and Recyclable Adsorbent for Highly Sensitive Simultaneous Determination of Three Tetracyclines Residues in Milk Samples. *J. Chromatogr. A* **2018**, *1568*, 1–7. [CrossRef]
20. Wei, J.; Chen, H.; He, J.; Huang, Z.; Qin, H.; Xiao, X.; Ni, H.; Chi, H.; He, J. Cobalt-Based N-Doped Bamboo-like Graphene Tubes with Enhanced Durability for Efficient Oxygen Reduction Reaction in Direct Borohydride Fuel Cell. *Carbon* **2023**, *201*, 856–863. [CrossRef]
21. Chen, T.; Dai, L. Macroscopic Graphene Fibers Directly Assembled from CVD-Grown Fiber-Shaped Hollow Graphene Tubes. *Angew. Chem.* **2015**, *127*, 15160–15163. [CrossRef]
22. Wu, G.; Li, X.; Zhang, Z.; Dong, P.; Xu, M.; Peng, H.; Zeng, X.; Zhang, Y.; Liao, S. Design of Ultralong-Life Li–CO2 Batteries with IrO2 Nanoparticles Highly Dispersed on Nitrogen-Doped Carbon Nanotubes. *J. Mater. Chem. A* **2020**, *8*, 3763–3770. [CrossRef]
23. Mo, R.; Tan, X.; Li, F.; Tao, R.; Xu, J.; Kong, D.; Wang, Z.; Xu, B.; Wang, X.; Wang, C.; et al. Tin-Graphene Tubes as Anodes for Lithium-Ion Batteries with High Volumetric and Gravimetric Energy Densities. *Nat. Commun.* **2020**, *11*, 1374. [CrossRef] [PubMed]
24. Luo, X.; Huang, J.; Wang, X.; Weng, M.; Cao, Y.; Min, Y. Template Free Preparation of Graphene Tubes from Polyimide Catalyzed by Calcium Carbonate. *Chem. Commun.* **2023**, *59*, 13321–13324. [CrossRef]
25. Couteau, E.; Hernadi, K.; Seo, J.W.; Thiên-Nga, L.; Mikó, C.; Gaál, R.; Forró, L. CVD Synthesis of High-Purity Multiwalled Carbon Nanotubes Using $CaCO_3$ Catalyst Support for Large-Scale Production. *Chem. Phys. Lett.* **2003**, *378*, 9–17. [CrossRef]
26. Kathyayini, H.; Nagaraju, N.; Fonseca, A.; Nagy, J.B. Catalytic Activity of Fe, Co and Fe/Co Supported on Ca and Mg Oxides, Hydroxides and Carbonates in the Synthesis of Carbon Nanotubes. *J. Mol. Catal. Chem.* **2004**, *223*, 129–136. [CrossRef]
27. Schmitt, T.C.; Biris, A.S.; Miller, D.W.; Biris, A.R.; Lupu, D.; Trigwell, S.; Rahman, Z.U. Analysis of Effluent Gases during the CCVD Growth of Multi-Wall Carbon Nanotubes from Acetylene. *Carbon* **2006**, *44*, 2032–2038. [CrossRef]
28. Feng, J.; Yin, Y. Self-Templating Approaches to Hollow Nanostructures. *Adv. Mater.* **2019**, *31*, 1802349. [CrossRef]
29. Gao, Y.; Zhang, W.; Yue, Q.; Gao, B.; Sun, Y.; Kong, J.; Zhao, P. Simple Synthesis of Hierarchical Porous Carbon from Enteromorpha Prolifera by a Self-Template Method for Supercapacitor Electrodes. *J. Power Sources* **2014**, *270*, 403–410. [CrossRef]
30. Liang, Q.; Shao, B.; Tong, S.; Liu, Z.; Tang, L.; Liu, Y.; Cheng, M.; He, Q.; Wu, T.; Pan, Y. Recent Advances of Melamine Self-Assembled Graphitic Carbon Nitride-Based Materials: Design, Synthesis and Application in Energy and Environment. *Chem. Eng. J.* **2021**, *405*, 126951. [CrossRef]
31. Yang, Y.; Liu, J.; Zhou, C.; Zhang, P.; Guo, S.; Li, S.; Meng, X.; Lu, Y.; Xu, H.; Ma, H.; et al. In Situ Self-Assembly Synthesis of Carbon Self-Doped Graphite Carbon Nitride Hexagonal Tubes with Enhanced Photocatalytic Hydrogen Evolution. *Int. J. Hydrogen Energy* **2019**, *44*, 27354–27362. [CrossRef]
32. Yan, S.C.; Li, Z.S.; Zou, Z.G. Photodegradation Performance of g-C3N4 Fabricated by Directly Heating Melamine. *Langmuir* **2009**, *25*, 10397–10401. [CrossRef] [PubMed]
33. Bian, S.-W.; Ma, Z.; Song, W.-G. Preparation and Characterization of Carbon Nitride Nanotubes and Their Applications as Catalyst Supporter. *J. Phys. Chem. C* **2009**, *113*, 8668–8672. [CrossRef]
34. Li, J.; Cao, C.; Zhu, H. Synthesis and Characterization of Graphite-like Carbon Nitride Nanobelts and Nanotubes. *Nanotechnology* **2007**, *18*, 115605. [CrossRef]
35. Mo, Z.; Xu, H.; Chen, Z.; She, X.; Song, Y.; Wu, J.; Yan, P.; Xu, L.; Lei, Y.; Yuan, S.; et al. Self-Assembled Synthesis of Defect-engineered Graphitic Carbon Nitride Nanotubes for Efficient Conversion of Solar Energy. *Appl. Catal. B Environ.* **2018**, *225*, 154–161. [CrossRef]
36. Mou, Z.; Chen, X.; Du, Y.; Wang, X.; Yang, P.; Wang, S. Forming Mechanism of Nitrogen Doped Graphene Prepared by Thermal Solid-State Reaction of Graphite Oxide and Urea. *Appl. Surf. Sci.* **2011**, *258*, 1704–1710. [CrossRef]
37. Vogel, W.; Hosemann, R. The Paracrystalline Nature of Pyrolytic Carbons. *Carbon* **1979**, *17*, 41–48. [CrossRef]
38. Cuesta, A.; Dhamelincourt, P.; Laureyns, J.; Martínez-Alonso, A.; Tascón, J.M.D. Raman Microprobe Studies on Carbon Materials. *Carbon* **1994**, *32*, 1523–1532. [CrossRef]

39. Frank, O.; Mohr, M.; Maultzsch, J.; Thomsen, C.; Riaz, I.; Jalil, R.; Novoselov, K.S.; Tsoukleri, G.; Parthenios, J.; Papagelis, K.; et al. Raman 2D-Band Splitting in Graphene: Theory and Experiment. *ACS Nano* **2011**, *5*, 2231–2239. [CrossRef]
40. Jiao, J.; Liu, X.; Gao, W.; Wang, C.; Feng, H.; Zhao, X.; Chen, L. Two-step Synthesis Flowerlike Calcium Carbonate/Biopolymer Composite Materials. *CrystEngComm* **2009**, *11*, 1886–1891. [CrossRef]
41. She, X.; Xu, H.; Wang, H.; Xia, J.; Song, Y.; Yan, J.; Xu, Y.; Zhang, Q.; Du, D.; Li, H. Controllable Synthesis of CeO_2/g-C_3N_4 Composites and Their Applications in the Environment. *Dalt. Transact.* **2015**, *44*, 7021–7031. [CrossRef] [PubMed]
42. Ewels, C.; Glerup, M.; Krstic, V.; Basiu, V.; Basiuk, E. Nitrogen and Boron Doping in Carbon Nanotubes. In *Chemistry of Carbon Nanotubes*; American Scientific Publishers: Stevenson Ranch, CA, USA, 2007; pp. 1–82.
43. She, X.; Xu, H.; Xu, Y.; Yan, J.; Xia, J.; Xu, L.; Song, Y.; Jiang, Y.; Zhang, Q.; Li, H. Exfoliated Graphene-like Carbon Nitride in Organic Solvents: Enhanced Photocatalytic Activity and Highly Selective and Sensitive Sensor for The Detection of Trace Amounts of Cu^{2+}. *J. Mater. Chem. A* **2014**, *2*, 2563–2570. [CrossRef]
44. Han, Q.; Wang, B.; Zhao, Y.; Hu, C.; Qu, L. A Graphitic-C3N4 "Seaweed" Architecture for Enhanced Hydrogen Evolution. *Angew. Chem. Int. Ed.* **2015**, *54*, 11433–11437. [CrossRef]
45. Sianipar, M.; Kim, S.H.; Iskandar, F.; Wenten, I.G. Functionalized Carbon Nanotube (CNT) Membrane: Progress and Challenges. *RSC Adv.* **2017**, *7*, 51175–51198. [CrossRef]